Separation Science and Technology
Publication details, including instructions for authors and subscription information:
http://www.informaworld.com/smpp/title~content=t713708471

Nonlinear Multicomponent Gradient Chromatography in Metal Affinity Systems

Suresh Vunnum; Venkatesh Natarajan; Stuart Gallant; Steven Cramer

To cite this Article Vunnum, Suresh , Natarajan, Venkatesh , Gallant, Stuart and Cramer, Steven(1998) 'Nonlinear Multicomponent Gradient Chromatography in Metal Affinity Systems', Separation Science and Technology, 33: 16, 2465 — 2489
To link to this Article: DOI: 10.1080/01496399808545314
URL: http://dx.doi.org/10.1080/01496399808545314

SEPARATION SCIENCE AND TECHNOLOGY, 33(16), pp. 2465–2489, 1998

Nonlinear Multicomponent Gradient Chromatography in Metal Affinity Systems

SURESH VUNNUM,* VENKATESH NATARAJAN,
STUART GALLANT,† and STEVEN CRAMER‡
DEPARTMENT OF CHEMICAL ENGINEERING
RENSSELAER POLYTECHNIC INSTITUTE
TROY, NEW YORK 12180-3590, USA

ABSTRACT

In this paper the metal affinity interaction chromatography (MAIC) model is employed in concert with appropriate mass transport equations to study preparative linear gradient chromatography in immobilized metal affinity chromatography (IMAC) systems. The MAIC model accounts for the nonlinear adsorption of proteins and mobile phase modulators (e.g., imidazole), and is shown to accurately predict gradient separations of proteins under overloaded conditions. Experimental and simulation results indicate that the concentration-dependent sorption of imidazole and protein–imidazole interference effects can severely deform linear gradients in IMAC systems. The steric accessibility and displacer characteristics of imidazole together with multicomponent interference effects can lead to unusual protein elution profiles and the spiking of imidazole between the feed components. Due to their ability to act as displacers, these imidazole spikes can sharpen protein tails, decreasing the interface shock layer thickness and improving resolution. Finally, iterative optimization schemes are employed to study the influence of the transient displacer characteristics of imidazole shocks on the optimum operating conditions.

INTRODUCTION

Linear gradient elution is widely employed in preparative chromatography (1–3). As the strength of the mobile phase increases in a linear fashion, the

* Present address: Purification Process Development Division, Genetics Institute Inc., One Burtt Road, N. Andover, MA 01810, USA.
† Present address: Bayer Corporation, 800 Dwight Way, Berkeley, CA 94701, USA.
‡ To whom correspondence should be addressed.

components of the feed solution are eluted from the column in their order of increasing affinity. Gradient elution allows components of widely varying chromatographic affinity to be concentrated and separated in a single chromatographic operation.

Immobilized metal affinity chromatography (IMAC) is a group-specific adsorption technique for the separation of biomolecules. The stationary phase in these systems consists of metal ions immobilized to a base resin using chelating agents such as iminodiacetic (IDA) acid. The exposed amino acid residues on the surface of a protein, such as the imidazole group of histidine, contribute to the binding of the protein to the immobilized metal ions. The metal ions typically employed in these systems include Cu(II), Zn(II), and Ni(II). The type of metal ion employed affects both the selectivity and the capacity of these systems.

IMAC systems offer many advantages vis-à-vis other chromatographic techniques based on affinity interactions. These systems are low cost, offer high capacities, employ mild elution conditions, and can be repeatedly stripped and reloaded with metal ions (4). Furthermore, it has been shown in these systems that proteins retain their biological activity after elution (5).

A number of analytical models have been presented for gradient chromatography (6, 7); however, such models do not consider the modulator sorption and assume a single protein eluting with a linear adsorption isotherm. Velayudhan and Ladisch (8) presented simulation results which account for nonlinear solute adsorption as well as modulator sorption in reversed phase systems. In IMAC, due to the high affinity of the traditionally employed mobile phase modulators (9) (e.g., imidazole), the quantification of the "protein–modulator" interference effects is crucial for the understanding of nonlinear protein separations.

Several researchers have employed Langmuir equilibria to describe IMAC systems (10, 11). However, the affinity constants determined using the Langmuir model are not adequate for predicting protein adsorption behavior as a function of modulator concentration. We have recently developed a metal affinity interaction chromatographic (MAIC) model which accounts for multiple-site interactions and the steric hindrance of stationary phase sites upon protein binding in IMAC systems (12). This model is able to account for differential saturation capacities as well as the modulator dependence of protein adsorption. The MAIC model has also been shown to accurately predict nonlinear protein adsorption behavior in IMAC systems (9, 12).

In this article, the MAIC model is employed in concert with mass transport equations to study the influence of "protein–modulator" interference effects on the operating conditions in preparative linear gradient IMAC systems. The behavior of these systems with and without imidazole in the equilibration buffer and the feed mixture are studied using simulations, and the results of these simulations are experimentally verified. The effects of having weakly

binding proteins in the feed mixture are then investigated using simulations. Subsequently, the model is employed for the optimization of nonlinear multicomponent gradient separations. Finally, the influences of the feed stream composition, solubility, and gap width constraints on these optimization results are examined.

THEORY

Multicomponent Equilibrium

The metal affinity interaction chromatographic (MAIC) model is a three-parameter model that incorporates mobile phase modulator effects and explicitly accounts for the multipointed nature of protein adsorption and the steric hindrance of the stationary phase sites upon binding of macromolecules. As a result, it is capable of accurately predicting multicomponent protein adsorption in IMAC systems. In this section we briefly review the model [for a detailed description see Vunnum et al. (12)].

Consider an immobilized Cu surface with a total capacity of Λ mM. Upon adsorption, the protein interacts with "n_i" sites on the stationary phase (number of interaction sites) and sterically hinders "σ_i" Cu sites (steric factor). These sterically hindered sites are unavailable for the binding of other macromolecules in free solution. On the other hand, the sterically hindered sites are accessible to relatively small mobile phase modulators such as imidazole. For a system of "N" proteins and a single mobile phase modifier, "$N + 1$" equilibrium expressions can be written to represent multicomponent binding equilibria. The equation representing the modulator binding equilibrium is

$$C_1 + Q_v \Leftrightarrow Q_1 \tag{1}$$

where the subscript "1" refers to the mobile phase modulator with a single coordination site, Q_v refers to the vacant sites on the stationary phase, C_1 refers to the mobile phase concentration of the modulator, and Q_1 is the stationary phase concentration of the modulator.

$$C_i + n_i\overline{Q}_v \Leftrightarrow Q_i, \qquad i = 2, 3, \ldots, N + 1 \tag{2}$$

Equation (2) describes the protein binding equilibrium. The subscript "i" refers to the proteins and $\overline{Q}_v$ represents the vacant sites on the stationary phase that are accessible for the adsorption of the proteins. C_i and Q_i represent the mobile phase and stationary phase concentrations, respectively, of the proteins. The equilibrium constant, K_i, for the modifier is given by

$$K_1 = \frac{Q_1}{C_1 Q_v} \tag{3}$$

and for the proteins is given by

$$K_i = \frac{Q_i}{C_i \overline{Q}_v^{n_i}} \tag{4}$$

Mass balance on the stationary phase yields

$$\Lambda = \overline{Q}_v + \overline{Q}_1 + \sum_{i=2}^{N+1} (n_i + \sigma_i) Q_i \tag{5}$$

where $\overline{Q}_1$ refers to the modulator bound to the sterically unshielded copper sites on the stationary phase, n_i is the number of interactions sites of solute i, and σ_i is the steric factor of solute i. Equations (3), (4), and (5) together define protein multicomponent equilibria on IMAC surfaces.

Mass Transport Equations

The model employed to describe mass transport in this work is a single parameter, lumped dispersion model. Equation (6) describes mass transport in the packed bed of a chromatography column:

$$-D_i \frac{\partial^2 C_i}{\partial Z^2} + U_0 \frac{\partial C_i}{\partial Z} + \frac{\partial C_i}{\partial t} + \frac{1 - \epsilon}{\epsilon} \frac{\partial Q_i}{\partial t} = 0 \tag{6}$$

where Z is the axial position, t is time, ϵ is the total porosity of the column, U_0 is the chromatographic velocity and is equal to U_s/ϵ, where U_s is the superficial velocity, and D_i represents an effective lumped dispersion coefficient which includes all transport limitations. The stationary phase is assumed to be in equilibrium with the mobile phase:

$$Q_i = F_i(C_1, C_2, \ldots, C_{N+1}) \tag{7}$$

The equilibrium expression F_i is the MAIC formalism discussed above. The above equations are solved in conjunction with the appropriate initial and boundary conditions which describe the gradient process.

Numerical Method

In order to solve this system of partial differential equations, a finite difference numerical technique developed by Czok et al. (13) was employed. In this technique a simple relation exists between the observed efficiency of the chromatography column, the effective dispersion coefficient of Eq. (6), and the dimensions of the finite difference grid:

$$\frac{H}{L} = \frac{2D_i}{LU_0} = \Delta z - \frac{1}{1 + k'} \Delta \tau \tag{8}$$

where H is the height equivalent to a theoretical plate, L is the column length, k' is the capacity factor, Δz is the step size in the spatial dimension, and $\Delta \tau$

is the dimensionless step size in the time dimension. Based on the observed plate height from experimental measurements, an effective dispersion coefficient of 2.0×10^{-2} cm^2/s was employed for the solutes in this study.

Chromatographic Optimization

Optimization involves the maximization or minimization of an objective function. In preparative chromatography the production rate of the process may be regarded as the objective function (14). The production rate of the ith component is defined as follows:

$$\mathrm{PR}_i = \frac{C_{i,\mathrm{f}} V_\mathrm{f} Y_i}{t_\mathrm{cyc} V_\mathrm{sp}} \tag{9}$$

where $C_{i,\mathrm{f}}$ is the feed concentration of the ith component, V_f is the feed volume, Y_i is the yield of the ith component, t_cyc is the cycle time, and V_sp is the stationary phase volume. Maximization of the production rate will allow the largest quantity of purified product to be produced in the shortest amount of time with the least amount of stationary phase.

The cycle time includes the time for column regeneration. In this study a regeneration time corresponding to 7 column dead volumes was assumed. Thus, the cycle time is defined as

$$t_\mathrm{cyc} = (\tau_\mathrm{f} + \tau_\mathrm{sep} + 7)t_0 \tag{10}$$

where τ_f and τ_sep are the dimensionless feed and separation times, respectively, and t_0 is the time taken by an unretained tracer to traverse the column.

The yield in the objective function is calculated from the formula

$$Y_i = \frac{\int_{t_1}^{t_2} C_i dt}{C_{i,\mathrm{f}} t_\mathrm{f}} \tag{11}$$

where t_f is the feed time, and the cut times, t_1 and t_2, are selected to maximize the yield at the specified purity.

Parameters

In this study the separation of an equal composition mixture of ribonuclease A (Rnase A) and myoglobin was optimized. The parameters in this problem are fixed quantities and include the capacity of the stationary phase, the initial imidazole concentration, pH, and the adsorption properties of the proteins.

Decision Variables

During optimization the values of the decision variables are selected to maximize the objective function. In this study the effects of two decision

variables, the feed time, t_f, and the gradient slope, G_{slope}, are considered. Manipulation of these variables allows the mass of protein purified per cycle and the time per cycle to be controlled. Proper selection of the feed volume and gradient slope will allow the largest amount of protein to be purified in the shortest amount of time.

Constraints

Most industrial processes have prespecified requirements (i.e., constraints on the variables of the problem). Four important constraints which are often imposed are: maximum protein concentration (to prevent precipitation or aggregation), purity, yield, and separation gap width. Maximum protein concentration is an example of a physical constraint on the process. In contrast, purity, yield, and separation gap width are all constraints that are defined by the efficiency of the purification system and by the desired quality of the product. In this study, constraints were set on the separation gap width, maximum protein concentration, purity, and yield.

Optimization Technique

The optimization technique employed in this manuscript was an iterative scheme adapted from the work of Gallant et al. (14). For a given feed volume and set of parameters and constraints, the iterative loop employed to optimize the gradient slope is shown in Fig. 1.

EXPERIMENTAL METHODS

Materials

Bulk chelating Superose (10 μm) containing covalently bound iminodiacetic acid (IDA) was donated by Pharmacia LKB Biotechnology (Uppsala, Sweden) and was packed in a 57 × 5 mm I.D. glass column. A strong cation exchange (SCX) (sulfopropyl, 8 μm, 50 × 5 mm I.D.) column was donated by Waters Chromatography (Milford, MA). Bulk BioSeries strong cation exchange (SCX) material (donated by Rockland Technologies, Newport, DE) was packed in a 250 × 4.6 mm I.D. column. POROS R/H reversed phase chromatographic column (100 × 4.6 mm I.D.) was donated by PerSeptive Biosystems (Cambridge, MA). Acetonitrile was purchased from Fisher Scientific (Fairlawn, NJ). Sodium chloride, sodium monobasic phosphate, sodium dibasic phosphate, sodium acetate, cupric sulfate, ethylenediamine tetraacetic acid (EDTA), imidazole, and all proteins were purchased from Sigma (St. Louis, MO).

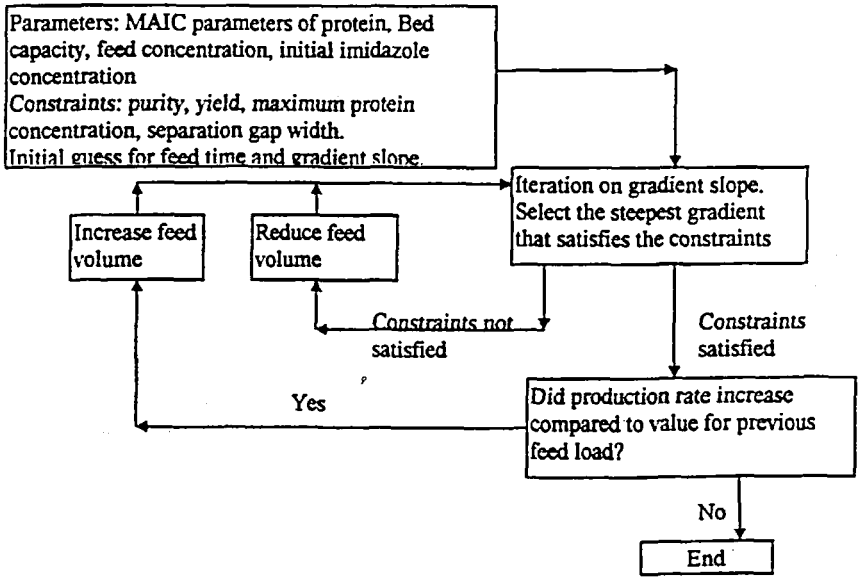

FIG. 1 Iterative scheme employed for optimization studies. Adapted from Ref. 14.

Apparatus

The system consisted of two Model P-500 pumps (Pharmacia, LKB) connected to the chromatographic column via a Model MV-7 injector (Pharmacia, LKB). Fractions of the column effluent were collected from the linear gradient chromatography experiments using a model 2212 Helirac fraction collector (Pharmacia, LKB). The collected fractions were subsequently analyzed for protein and imidazole concentrations. A Spectroflow 757 UV-VIS absorbance detector (Applied Biosystems, Foster City, CA) was employed to monitor the column effluent, and a model C-R3A Chromatopac integrator (Shimadzu, Kyoto, Japan) was employed for data acquisition and analysis.

Immobilization of Cu^{2+}

The IDA column was washed with 10 column volumes of distilled water and subsequently loaded with copper ions by equilibration with an aqueous solution of 0.3 M copper sulfate, pH 3.9. Unadsorbed metal ions were removed by perfusing the IDA-Cu(II) column with 5 column volumes of 0.1 M sodium acetate, pH 4.0. The column was then washed with 3 column volumes of distilled water and equilibrated with the appropriate buffer solution.

Determination of MAIC Parameters

The linear adsorption parameters of the proteins, the number of interaction sites (n_i), and the equilibrium constant (K_i) were estimated from linear elution experiments at various imidazole concentrations. The steric factors (σ_i) of the proteins were obtained from nonlinear frontal experiments carried out over a range of imidazole concentrations. The MAIC parameters of imidazole were obtained by fitting the isotherm data points to the single component Langmuir expression. For a detailed discussion of these parameter estimation techniques, the reader is referred to Vunnum et al. (12).

Linear Gradient Chromatography of Proteins

The column was initially equilibrated with Carrier A (0.5 mM imidazole, 0.5 M NaCl, 50 mM sodium phosphate, pH 7.0). The feed solution was subsequently loaded onto the column. After an appropriate feed volume was loaded, a linear gradient from Carrier A to Carrier B (30 mM imidazole, 0.5 M NaCl, 50 mM sodium phosphate, pH 7.0) was initiated. All the experiments were carried out at room temperature at a flow rate of 0.2 mL/min. Fractions were collected directly from the column effluent and analyzed as described below. Details of the individual experiments are given in the figure legends.

Regeneration

While these columns can be readily regenerated using several column volumes of 30 mM imidazole, in the experiments shown in this paper extra precaution was taken to ensure that the total bed capacity remained constant in these experiments. Accordingly, the column was then washed with 10 column volumes of deionized water and stripped of Cu^{2+} ions by perfusing with 5 column volumes of 0.1 M EDTA, followed again by washing with 10 column volumes of deionized water. The immobilization of Cu^{2+} was then carried out as described above.

Effluent Analysis by HPLC

Effluent fractions obtained from the frontal chromatography experiments were diluted 5–100-fold, and 25-μL samples were analyzed using the following methods.

Imidazole Analysis. Isocratic chromatography was performed on a 250 × 4.6 mm I.D. SCX column using a carrier of 15 mM phosphate buffer, pH 5.0, and a flow rate of 0.9 mL/min. The column effluent was monitored at 400 nm.

Ribonuclease A Analysis. Isocratic chromatography was performed on a 50 × 5 mm I.D. SCX column using a carrier of 50 mM phosphate

buffer, pH 6.0, containing 60 mM NaCl and a flow rate of 0.5 mL/min. The column effluent was monitored at 280 nm.

Myoglobin Analysis. Isocratic chromatography was performed on a 100 × 4.6 mm I.D. POROS reversed phase column using a carrier of 38% (v/v) acetonitrile in 50 mM phosphate buffer, pH 2.2, at a flow rate of 0.9 mL/min. The column effluent was monitored at 280 nm.

RESULTS AND DISCUSSION

The model was first employed to examine the behavior of these systems when there was no imidazole in the equilibration buffer or the feed mixture. Figure 2 shows simulations of the separation of Rnase A and myoglobin employing various gradient slopes of imidazole. (*Note*: The MAIC parameters employed in these simulations are presented in Table 1.) The concentration-dependent sorption of imidazole and the concave downward nature of its adsorption isotherm leads to the formation of an imidazole shock layer at the front of the gradient. In addition, the nonlinear competition for the stationary phase sites between the proteins and the imidazole leads to further deformation of the linear gradient. Figure 2(a) shows the elution profile of the Rnase A–myoglobin separation employing an imidazole gradient of 0.25 mM per column volume. Since imidazole exhibits concentration-dependent displacer characteristics (9), the imidazole shocks lead to the displacement of certain proteins. Under these conditions, myoglobin elutes in the imidazole zone while the imidazole shock effectively displaces Rnase A. Figures 2(b) and 2(c) show the simulation results of this separation at gradient slopes of 1 and 2 mM per column volume, respectively. At a gradient slope of 2 mM the imidazole shock is strong enough to effectively displace both Rnase A and myoglobin (Fig. 2c), while a slope of 1 mM results in a transient desorption of myoglobin (Fig. 2b). (*Note*: In other words, given sufficient length of column, under the same gradient slopes as in Figs. 2a and 2b, myoglobin would also eventually be displaced ahead of the imidazole shock as in Fig. 2c.) This is because 1) the imidazole concentration across the shock is an increasing function of column length and 2) for a given protein there exists a critical concentration beyond which imidazole will effectively displace the protein ahead of its front (9).

The model was next employed to examine the behavior of these systems when the equilibration buffer and the feed mixture contained imidazole. It turns out that the nonlinear competition for the stationary phase sites between the protein and the imidazole can lead to significant system peaks in these separations. The elution profiles of the Rnase A–myoglobin separation when the column is initially equilibrated with a finite imidazole concentration are shown in Fig. 3. In contrast to the results shown in Fig. 2, when there is

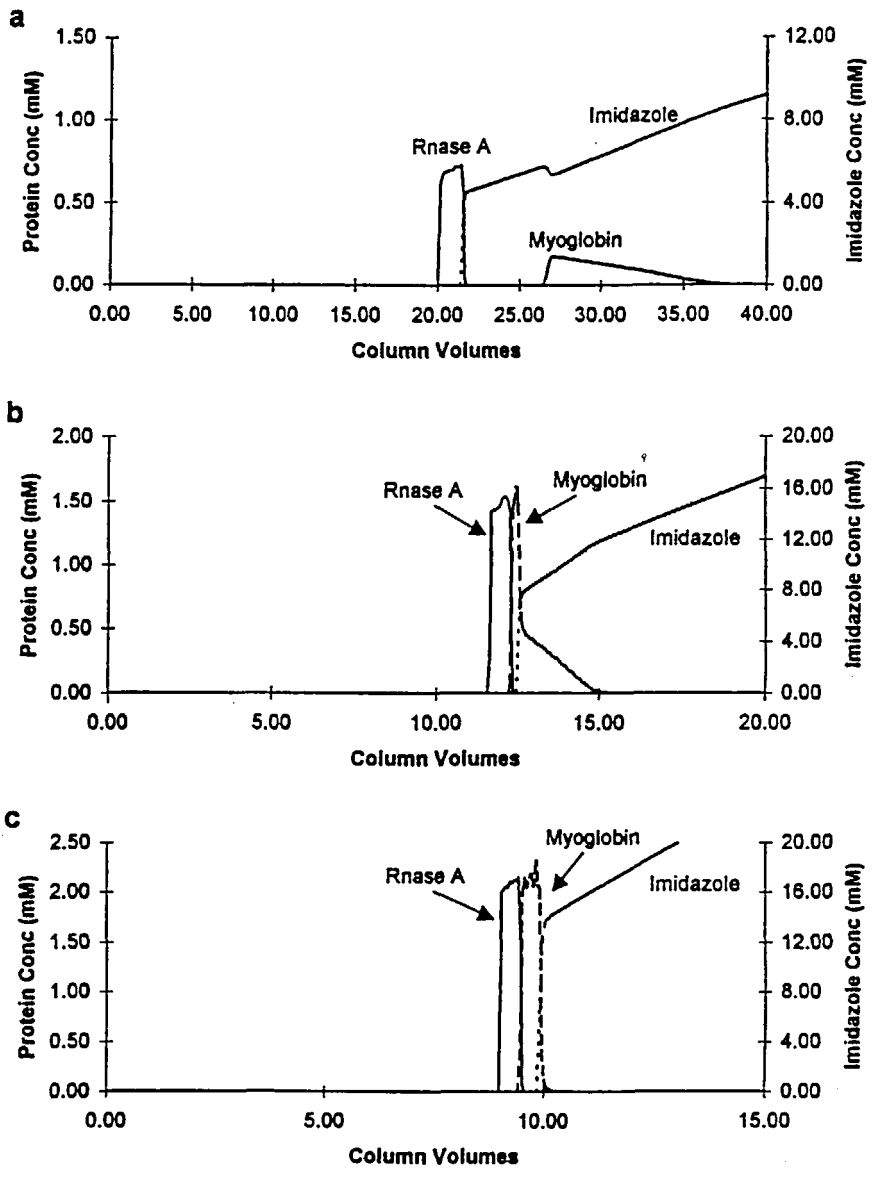

FIG. 2 Effect of gradient slope on the concentration change across the modulator shock and the modulator-induced displacement effects. Feed: 2 column volumes of 0.5 mM each of Rnase A and myoglobin. Gradient slope: (a) 0.25 mM per column volume, (b) 1 mM per column volume, and (c) 2 mM per column volume.

TABLE 1
MAIC Adsorption Parameters[a]

Solute	Interaction sites n_i	Equilibrium constant K_i	Steric factor σ_i
Ribonuclease A	1.81 ± 0.05	2.1×10^{-1}	4.1 ± 0.4
Myoglobin	3.3 ± 0.4	6.6×10^{-2}	3.0 ± 0.7
Conalbumin	4.7 ± 0.4	3.0×10^{-5}	16 ± 1
Lysozyme	1.5 ± 0.1	3.5×10^{-2}	—[b]
Ovalbumin	2.7 ± 0.2	6.0×10^{-4}	1.8 ± 0.1
Imidazole	1.0	3.55	0.0

[a] Phase ratio: 0.24. Bed capacity (Λ): 201.45 mM.
[b] Not estimated due to solubility constraints. A value of 8.0 has been assumed for the simulation shown in Fig. 7.

imidazole initially in the column, the linear gradient is not subjected to as severe a shock formation. Furthermore, the adsorption of the feed proteins during loading leads to an induced imidazole step increase (Fig. 3a).

The effect of an increased gradient slope on this separation is shown in Fig. 3(b). The steeper imidazole gradient leads to the formation of prominent negative imidazole "system peaks" which coelute with the proteins and produce highly concentrated, narrow bands. In addition, this type of separation can lead to scenarios where the positive imidazole system peak ahead of the protein zone is completely engulfed by the shock formation at the front end of the gradient (Figs. 3b and 3c). While the magnitude of the change in the imidazole concentration across the shock is comparable to those shown in Fig. 2, under these conditions (i.e., when the column is initially equilibrated with imidazole), proteins cannot be displaced by the imidazole shock.

Figure 3(c) shows the influence of the feed load on the gradient separation. The feed volume in this simulation is three times that shown in Fig. 3(b), while the gradient slope is the same in both cases. As can be seen from these figures, increasing the feed volume leads to a dramatically different elution profile under identical gradient conditions. The gradient is severely deformed under these conditions and the complex imidazole system peaks lead to a multiple peak profile of Rnase A with a sharp rear of the peak. In addition, the myoglobin concentration is higher than that in Fig. 3(b) due to the transient displacement effect of the imidazole shock layer.

In order to confirm that the theory was predicting the experimental behavior, a comparison was carried out for the Rnase A–myoglobin separation under conditions where the column was initially equilibrated with an imidazole concentration of 0.5 mM (Fig. 4). After loading the feed mixture in 0.5 mM imidazole, a linear gradient of 1 mM imidazole per column volume was

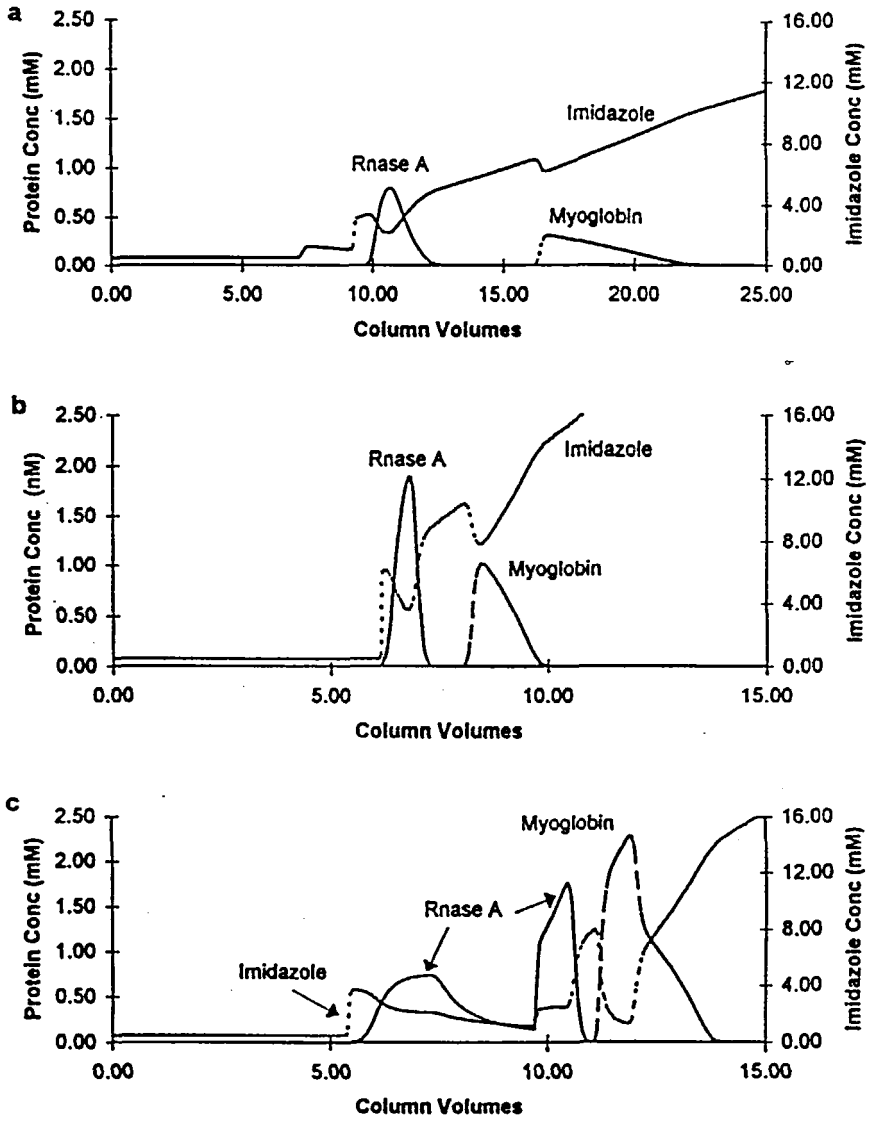

FIG. 3 System peaks in linear gradient chromatography. Feed composition: 0.5 mM each of Rnase A and myoglobin in 0.5 mM imidazole. (a) Feed: 2 column volumes; gradient slope: 0.5 mM per column volume. (b) Feed: 2 column volumes; gradient slope: 2 mM per column volume. (c) Feed; 6 column volumes; gradient slope: 2 mM per column volume.

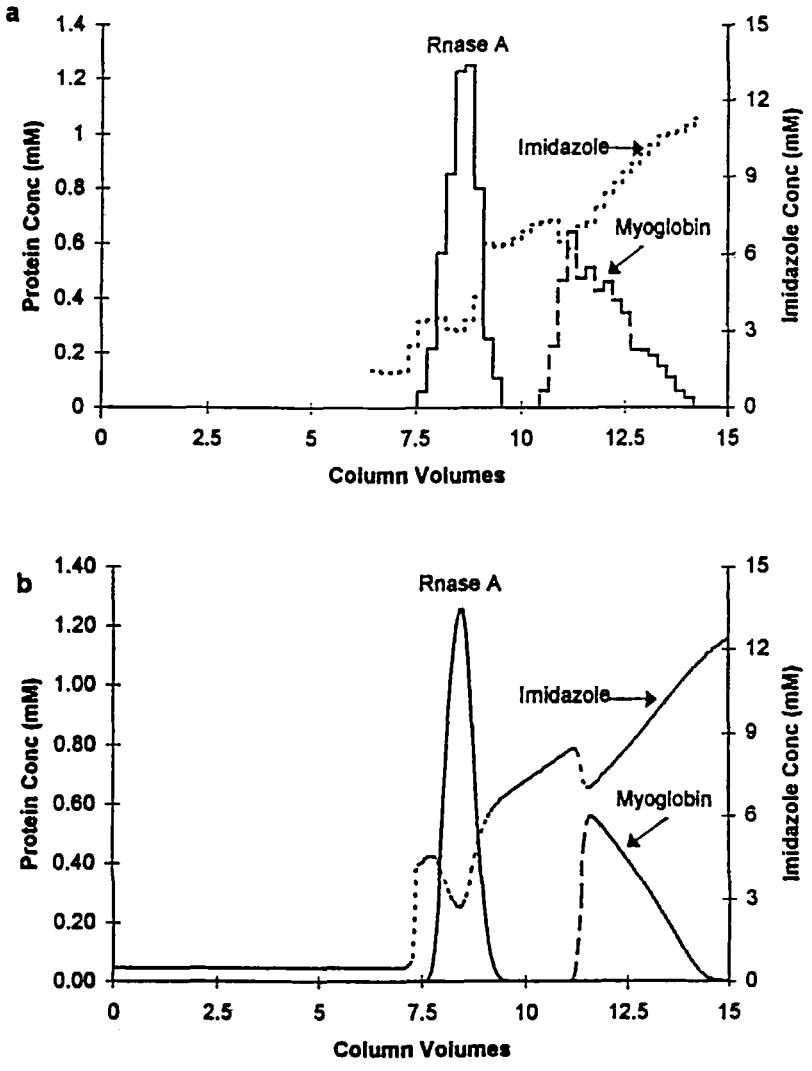

FIG. 4 Comparison of simulation and experimental chromatograms. (a) Experimental profile. (b) Simulation result. Feed: 2 column volumes of 0.5 mM each of Rnase A and myoglobin in 0.5 mM imidazole. Gradient slope: 1 mM per column volume.

employed. As can be seen from these figures, the concentrations of the positive and negative imidazole system peaks and the protein elution bands are well quantified. Further, the elution volumes of the proteins are in close agreement with the model prediction.

Figure 5 shows the experimental result and the theoretical prediction of this separation under identical gradient conditions as in Fig. 4, but with 2.5 times the feed volume. As in Fig. 4, the model does a good job of capturing the salient features of this complex elution profile. The results presented in Figs. 4 and 5 indicate that the MAIC model is indeed capable of describing complex behavior in nonlinear IMAC gradient systems.

The presence of weakly binding proteins in the feed mixture can dramatically alter the elution profiles in IMAC gradient systems. The elution profile of a gradient separation of conalbumin (a weakly retained protein), Rnase A, and myoglobin is shown in Fig. 6(a). As seen in the figure, the imidazole gradient is severely deformed, and the earlier eluting protein, conalbumin, coelutes with the induced imidazole step increase. Figures 6(b) and 6(c) illustrate the influence of the gradient slope on this separation. As can be seen in these figures, while the elution times of the other proteins are dependent on the gradient slope, the conalbumin retention time is not. This is due to the fact that the conalbumin adsorption isotherm is very sensitive to imidazole concentration, resulting in elution in the induced step increase.

Focusing of protein shocks in the presence of mobile phase modifiers can sometimes be detrimental to separations. Figure 7 shows the linear gradient separation of lysozyme, ovalbumin, and Rnase A at an initial imidazole concentration of 0.5 mM. Lysozyme and ovalbumin are weakly binding proteins and elute in the induced imidazole step increase. As seen in Fig. 7, the weakly retained proteins are focused at the induced imidazole step, resulting in a significant overlap of their bands. Further, the linear gradient undergoes a shock formation, resulting in a "bracketing" of lysozyme and ovalbumin between this shock and the induced imidazole step increase. Thus, despite a reasonable linear separation factor between lysozyme and ovalbumin, gradient chromatography, under these conditions, is unable to resolve the two proteins due to complex imidazole system peaks. It is important to note that this behavior would not be predicted from other isotherm models such as the Langmuir model.

Figure 8 shows the dependence of the linear retention of Rnase A and conalbumin on imidazole concentration (C_1). The data indicate that these proteins exhibit a selectivity reversal in the imidazole concentration range that was employed in Fig. 6. However, as was shown in Fig. 6, a good separation was achieved with an imidazole gradient in this range. Clearly, the selectivity in these systems is more complex than can be ascertained by simply examining linear retention plots. Thus, this precludes generalizations based

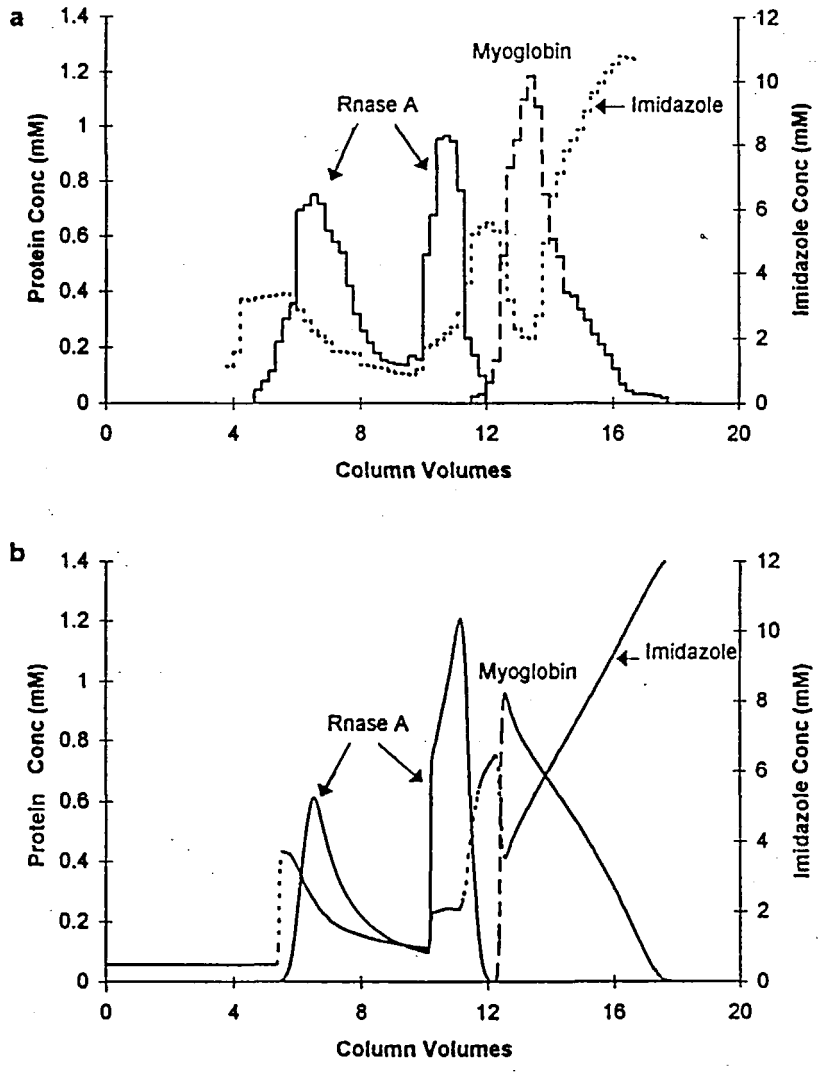

FIG. 5 Comparison of simulation and experimental chromatograms. (a) Experimental profile. (b) Simulation result. Feed: 5 column volumes of 0.5 mM each of Rnase A and myoglobin in 0.5 mM imidazole. Gradient slope: 1 mM per column volume.

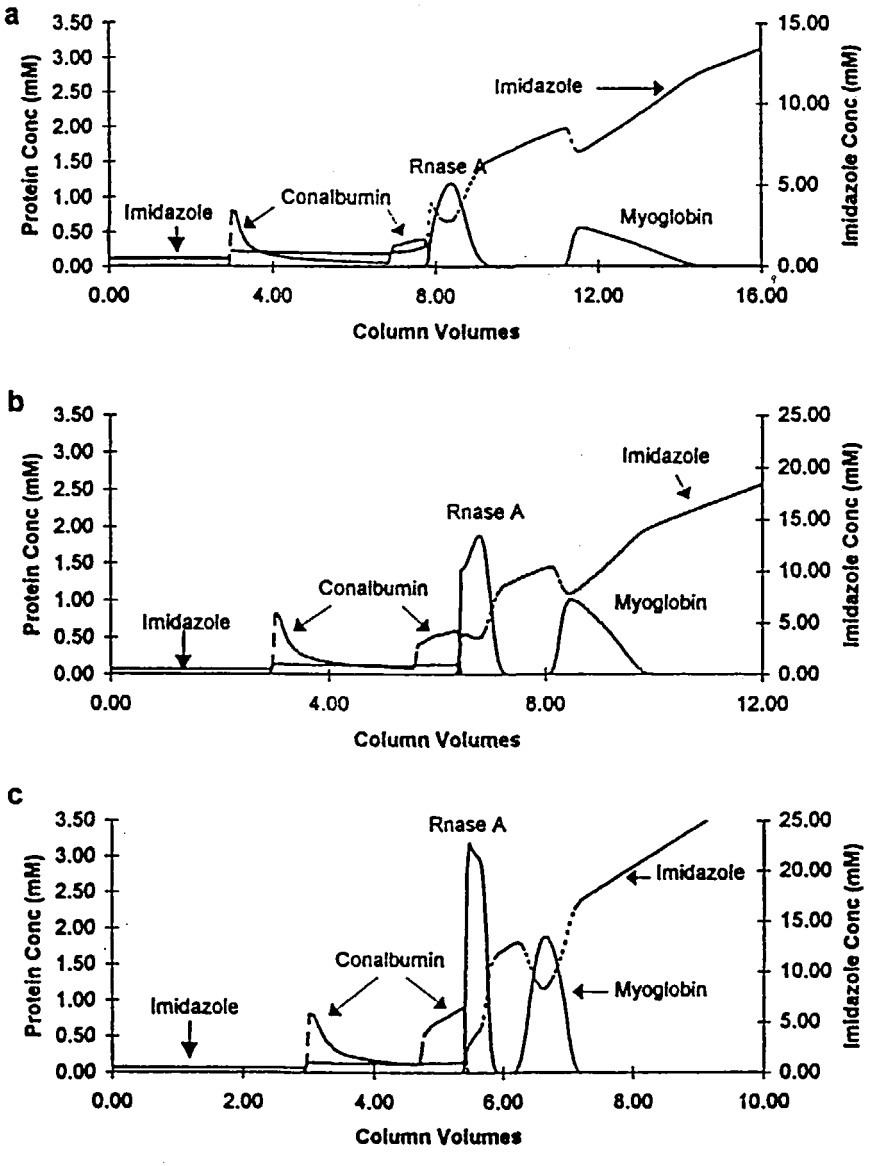

FIG. 6 Elution profiles of conalbumin containing feed mixtures. Feed: 2 column volumes of 0.5 mM of each protein in 0.5 mM imidazole. Gradient slope: (a) 1 mM per column volume, (b) 2 mM per column volume, and (c) 4 mM per column volume.

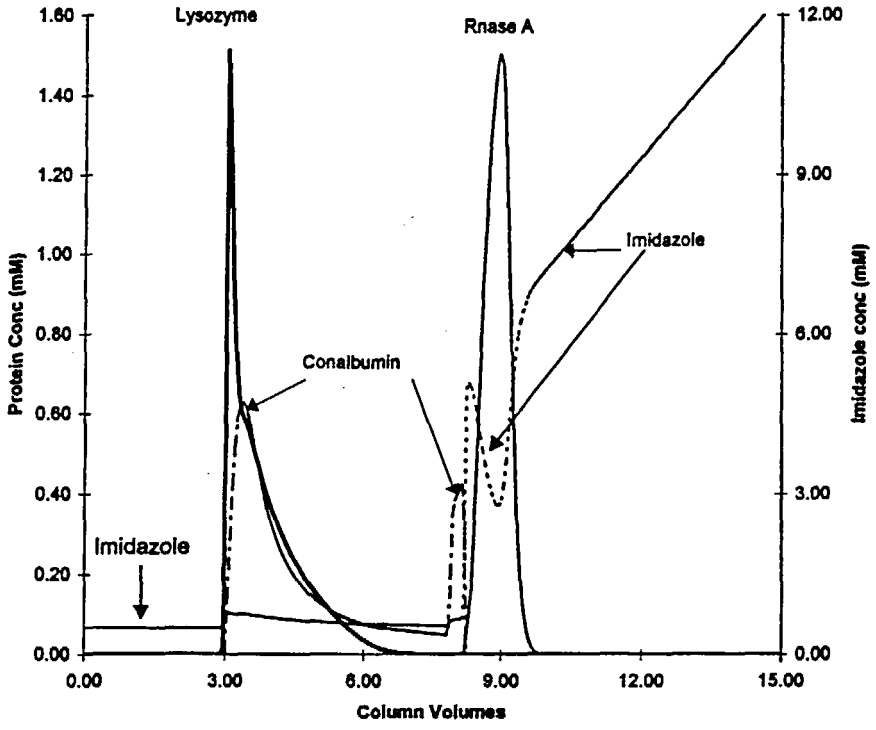

FIG. 7 Separation of weakly binding proteins. Feed: 0.5 mM each of ovalbumin, lysozyme, and Rnase A in 0.5 mM imidazole. Gradient slope: 1 mM per column volume.

on converging and diverging linear retention plots such as has been put forth for ion exchange and reversed phase systems (14, 15).

Optimization of Gradient Separations

In addition to employing the model to examine some of the complex behavior in nonlinear IMAC gradient systems, the model can also be used to identify operating conditions that lead to an optimum production rate for a given separation. The iterative scheme shown in Fig. 1 was used for identifying optimum gradient conditions for the separation of an equal composition feed mixture of Rnase A and myoglobin. This analysis was carried out with a separation gap constraint of 0.5 column dead volumes and with no constraint on the maximum protein concentration. Figure 9(a) shows the optimum imidazole gradient that produces the highest production rate of myoglobin at various feed volumes. As expected, the optimum gradient slope decreases with

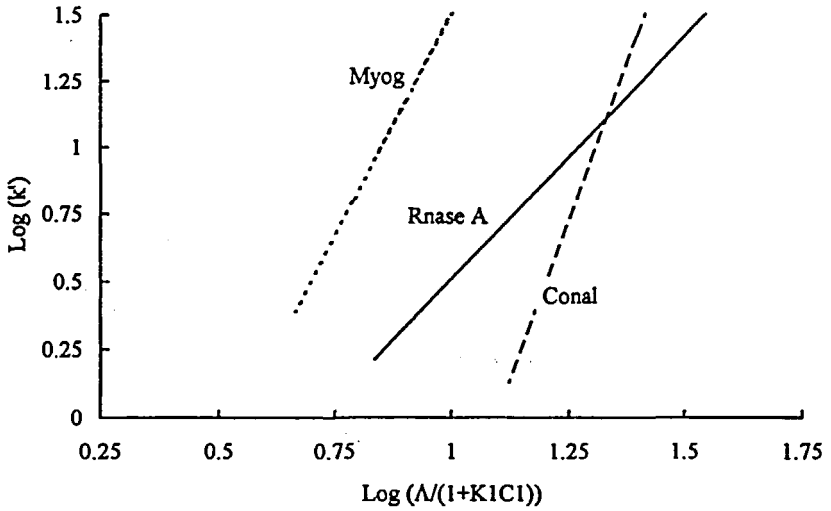

FIG. 8 Log k' plots. C_1 = imidazole concentration (mM).

increasing feed volume. The purity and yield are both 100% due to the separation gap constraint. Figure 9(a) also shows the influence of the initial imidazole concentration on the optimum gradient slope. Rnase A–myoglobin have a linear selectivity that is higher at lower imidazole concentration (Fig. 8). Hence, it would be expected that the optimum gradient slope for this separation would be higher when the initial imidazole concentration is lower. Surprisingly, the results at an initial imidazole concentration of 1.5 mM are higher than those at 0.5 and 5 mM. Thus, the results suggest the existence of an optimum initial imidazole concentration for these types of separations. Figure 9(b) shows the optimum production rate for this separation as a function of the feed volume. As seen in the figure, the production rate initially increases, reaches a plateau, and then declines with increasing feed volume. This is because the optimum gradient slope decreases with an increase in feed volume, resulting in longer separation times. The maximum production rate is 0.24 mmol/mL·min and is obtained at a feed volume of 5, with an initial imidazole concentration of 1.5 mM. Again, the data suggest a significant effect of the initial imidazole concentration.

Figures 10(a), 10(b), and 10(c) examine the effect of initial imidazole concentration on the effluent profile. The simulated chromatograms at initial imidazole concentrations of 1.5, 0.5, and 5.0 mM are shown in Figs. 10(a), 10(b), and 10(c), respectively. As seen in these figures, the gradient deforma-

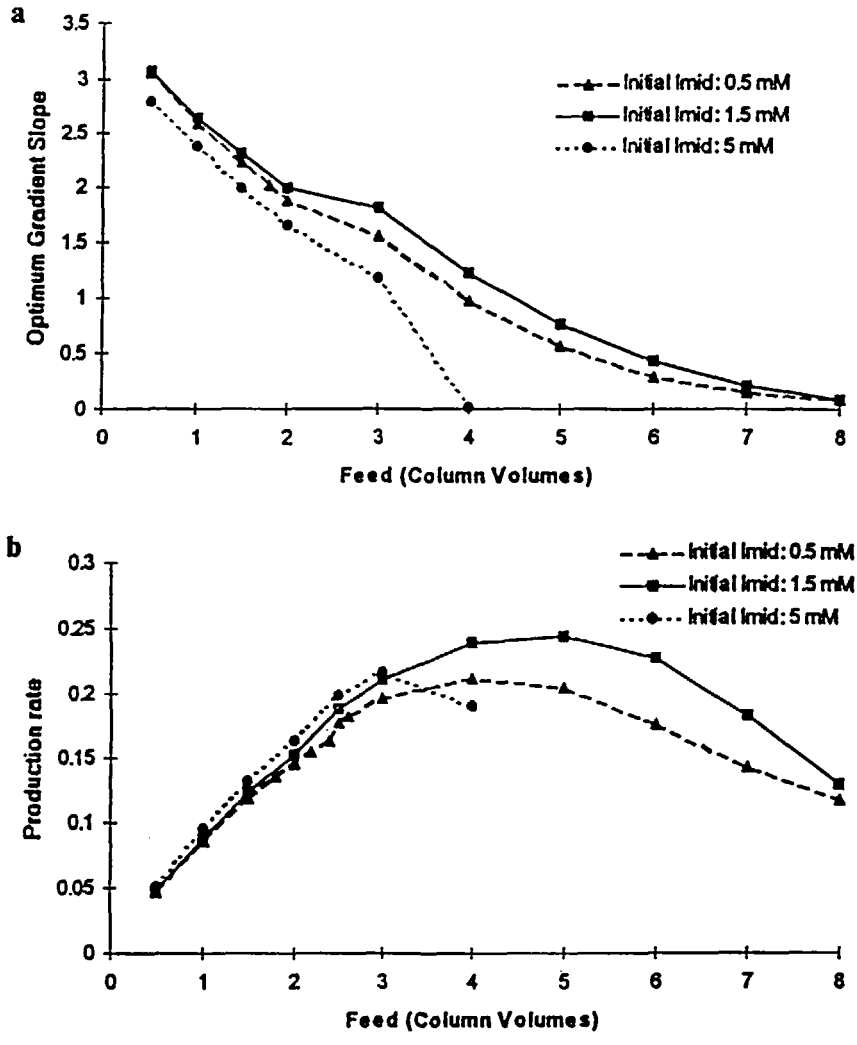

FIG. 9 Influence of initial imidazole concentration on the (a) optimum gradient slopes and (b) production rate for the Rnase A–myoglobin separation under a 0.5-column volume gap width constraint and no solubility constraint. Protein feed consists of 0.5 mM of each protein.

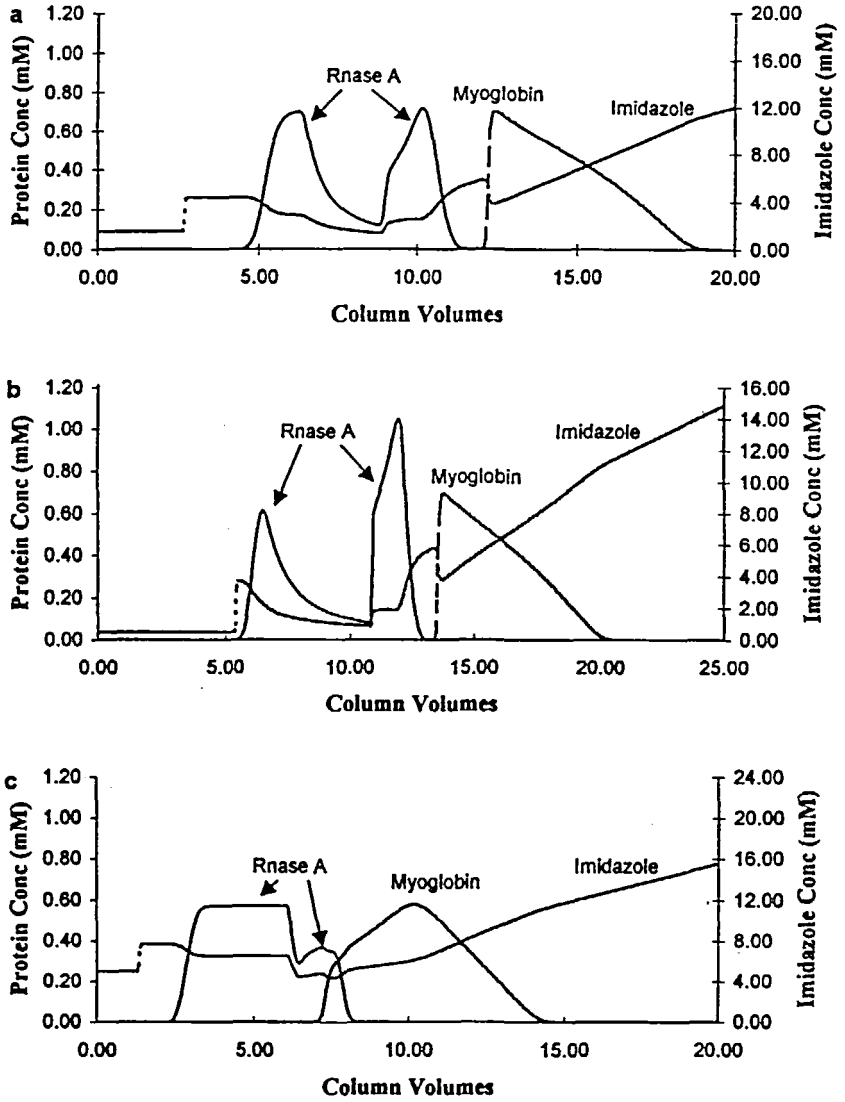

FIG. 10 Effect of initial imidazole concentration on the linear gradient separation of Rnase A–myoglobin. Feed: 5 column volumes of 0.5 mM of each protein in the corresponding equilibration imidazole concentration. Gradient slope: 0.758 mM per column volume. Initial imidazole concentration: (a) 1.5 mM, (b) 0.5 mM, and (c) 5 mM.

tion is more severe at lower initial imidazole concentration. At an initial imidazole concentration of 1.5 mM, the gap width constraint is satisfied (Fig. 10a). At an initial imidazole concentration of 0.5 mM (Fig. 10b), the strong gradient deformation results in a separation gap smaller than 0.5 column volumes and thus, the gradient slope would have to be *lowered* to satisfy the gap width constraint. On the other hand, at the higher initial imidazole concentration of 5 mM (Fig. 10c), the protein adsorption is highly attenuated. Furthermore, the positive influence of the displacement effect of the imidazole shock is not taken advantage of, since the gradient deformation is minimal under these conditions. Thus, in order to satisfy the gap width constraint of 0.5 column volumes under these conditions, the gradient slope would have to be *increased.*

Effect of Feed Stream Composition

Gradient deformation due to protein–imidazole interference effects is sensitive to the concentration and composition of the feed components. Further, the displacement effect of the imidazole shocks is generally a transient phenomenon. Thus, the feed stream composition and concentration can have a major impact on the selection of the optimum operating conditions.

Figures 11(a) and 11(b) show simulations of the separation of 2 column volumes of a 1:9 and 9:1 feed mixture of Rnase A–myoglobin, respectively. The gradient slope employed in these simulations is the optimum that satisfies a gap constraint of 0.5 column volumes. The significant difference in the optimum gradient slope shown in these figures arises primarily due to the nonlinear adsorption of myoglobin. In the case of a 1:9 feed mixture (Fig. 11a), the front of the myoglobin peak elutes approximately 6 columns ahead of its rear. This places a greater restriction on the maximum imidazole slope that can be selected. On the other hand, for the 9:1 feed mixture, a steeper gradient could readily be chosen since this separation can take advantage of the displacer characteristics of the imidazole shock.

Gap Width and Solubility Constraints

The optimum production rate curves with and without the gap width constraint are shown in Fig. 12 as a function of the feed volume. With a finite gap width constraint the production rate increases with feed volume up to a certain point, after which the production rate decreases. This is due to the fact that at higher feed volumes the optimum gradient slope must decrease in order to satisfy the gap width constraint. Relaxing the separation gap constraint leads to touching band profiles. Under these conditions, sample displacement can have a significant effect on the separation. As can be seen in Fig. 12, the production rate for separations with no gap constraint continues

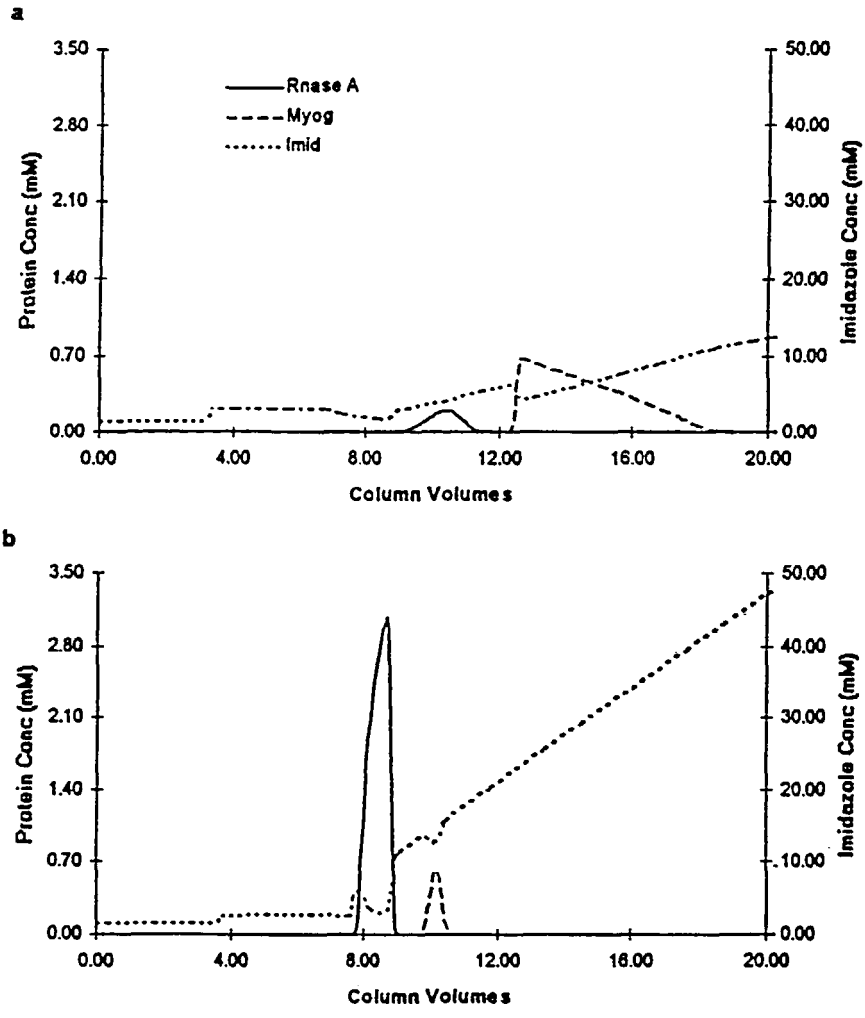

FIG. 11 Effect of feed composition on the optimum gradient slope under a gap width constraint of 0.5 mM. (a) Feed: 2 column volumes of 0.05 mM Rnase A and 0.45 mM myoglobin in 1.5 mM imidazole (feed ratio 1:9); gradient slope: 0.784 mM per column volume. (b) Feed: 2 column volumes of 0.45 mM Rnase A and 0.05 mM myoglobin in 1.5 mM imidazole (feed ratio 9:1); gradient slope: 3.26 mM per column volume.

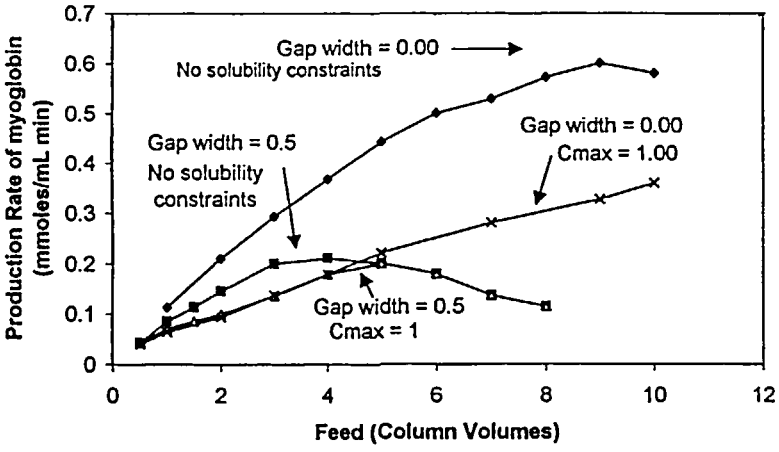

FIG. 12 Comparison of the production rates for the Rnase A–myoglobin separation under various optimization conditions. In all four cases the yield and purity constraints were 99.5% and 99%, respectively, and the initial imidazole concentration was 0.5 mM.

to increase well after the gap constraint separation has reached its maximum. Thus, preparative IMAC separations that include displacement effects will be able to separate significantly more protein per unit time, provided the yield and purity constraints are satisfied. These results are in qualitative agreement with prior results which indicated that sample displacement effects could substantially increase the chromatographic productivity of preparative linear gradient ion exchange systems (14).

A solubility constraint can also have a significant impact on the optimization results. Separations with both a gap width and a 1-mM solubility constraint (denoted by triangles in Fig. 12) result in lower production rates than those separations with a gap width constraint alone (denoted by squares in Fig. 12) at relatively low feed volumes. At higher feed volumes the gap width becomes the dominant constraint and the two curves coincide. The incorporation of the solubility constraint for the case with no gap constraint (denoted by crosses in Fig. 12) results in lower production rates than those with no solubility and gap constraints (denoted by diamonds in Fig. 12). However, the production rates are still significantly higher under these sample displacement conditions than those obtained with a finite gap width constraint.

CONCLUSIONS

In this paper the MAIC model has been shown to accurately account for the nonlinear adsorption of proteins and the mobile phase modifier in linear

gradient chromatography. The model has been employed to investigate deformation of linear gradients in IMAC systems and the unusual chromatographic behavior of proteins that result from multicomponent interference effects and the displacer characteristics of imidazole. It has been demonstrated in this article that the selectivity in these systems is more complex than can be ascertained by simply examining linear retention plots. In addition, iterative optimization schemes were employed to study optimum operating conditions for linear gradient IMAC systems under various conditions. The choice of the constraints to be imposed on the system has a profound effect on the optimum conditions. While the imposition of a gap width constraint results in an optimum initial imidazole concentration, relaxation of this constraint results in sample displacement effects and a marked improvement in the production rates in these systems. These results demonstrate that the MAIC model is well suited for aiding in the methods development and optimization of protein purification in preparative linear gradient IMAC systems.

NOMENCLATURE

C	mobile phase concentration (mM)
D	axial dispersion coefficient (cm^2/s)
H	height equivalent to a theoretical plate (cm)
k'	capacity factor
K	equilibrium constant (mM^{-n})
L	length of column (cm)
n	number of interaction sites
Q	stationary phase concentration (mM)
Q_v	concentration of vacant sites on the stationary phase (mM)
Q_v	concentration of vacant sites accessible to proteins (mM)
U_0	chromatographic velocity (cm/min)
U_s	superficial velocity (cm/min)
t	time (min)
t_0	hold-up time (min)
V_f	feed volume (mL)
V_{sp}	volume of stationary phase (mL)
Y	yield
Z	axial distance along column (cm)

Greek letters

ϵ	total porosity
Λ	bed capacity (mM)
σ	steric factor

τ dimensionless time ($= t/t_0$)

Subscripts

i component number
f feed

REFERENCES

1. S. Yamamoto, M. Nomura, and Y. Sano, *J. Chromatogr.*, *409*, 101–110 (1987).
2. L. R. Snyder, G. B. Cox, and P. E. Antle., *Ibid.*, *444*, 303–324 (1988).
3. F. D. Antia and Cs. Horvath, *Ibid.*, *484*, 1–27 (1989).
4. F. H. Arnold, *Bio/Technology*, *9*, 151–156 (1991).
5. B. Lonnerdal, J. Carlsson, and J. Porath, *FEBS Lett.*, *75*(1), 89–92 (1977).
6. D. D. Frey, *Biotech. Bioeng.*, *35*, 1055–1061 (1990).
7. G. Carta and W. B. Stringfield, *J. Chromatogr.*, *605*, 151–159 (1992).
8. A. Velayudhan and M. R. Ladisch, *Anal. Chem.*, *63*, 2028–2032 (1991).
9. S. Vunnum, S. R. Gallant, and S. M. Cramer, *Biotechnol. Prog.*, *12*, 84–91 (1996).
10. M. Belew, T. T. Yip, L. Andersson, and J. Porath, *J. Chromatogr.*, *403*, 197–206 (1987).
11. T. W. Hutchens and T. T. Yip, *Anal. Biochem.*, *191*, 160–168 (1990).
12. S. Vunnum, S. R. Gallant, Y. Kim, and S. M. Cramer, *Chem. Eng. Sci.*, *50*, 1785–1803 (1995).
13. M. Czok and G. Guiochon, *Anal. Chem.*, *62*, 189–200 (1990).
14. S. Gallant, S. Vunnum, and S. M. Cramer, *J. Chromatogr.*, *725*, 295–314 (1996).
15. A. Felinger and G. Guiochon, *Biotechnal. Prog.*, *12*, 638–644 (1996).

Received by editor January 23, 1998
Revision received April 1998